π-Splicer: Perceiving Accurate CSI Phases with Commodity WiFi Devices

Hongzi Zhu, *Member, IEEE*, Yiwei Zhuo, Qinghao Liu, and Shan Chang, *Member, IEEE*

Abstract—WiFi technology has gained a wide prevalence for not only wireless communication but also pervasive sensing. A wide variety of emerging applications leverage accurate measurements of the Channel State Information (CSI) information obtained from commodity WiFi devices. Due to hardware imperfection of commodity WiFi devices, the frequency response of internal signal processing circuit is mixed with the real channel frequency response in passband, which makes deriving accurate channel frequency response from CSI measurements a challenging task. In this paper, we identify non-negligible non-linear CSI phase errors and report that IQ imbalance is the root source of non-linear CSI phase errors. We conduct intensive analysis on the characteristics of such non-linear errors and find that such errors are prevalent among various WiFi devices. Furthermore, they are rather stable along time and the received signal strength indication (RSSI) but sensitive to frequency bands used between a transmission pair. Based on these key observations, we propose new methods to compensate both non-linear and linear CSI phase errors. We demonstrate the efficacy of the proposed methods by applying them in CSI splicing and indoor distance ranging. Results of extensive real-world experiments indicate that accurate CSI phase measurements can significantly improve the performance of splicing and the stability of the derived power delay profiles (PDPs). Moreover, the estimated distance errors are reduced by 5.7 times on average comparing to the state-of-the-art schemes.

Index Terms—Channel state information (CSI), non-linear phase error, rotation phase error, CSI splicing, indoor distance ranging

✦

1 INTRODUCTION

UBIQUITOUS WiFi technology has fostered a broad range of applications beyond a vehicle for communication. In recent years, a myriad of emerging applications, such as seeing through-walls [1], gesture recognition [2], [3], [4], line-of-sight (LOS) identification [5], [6], [7], indoor localization [8], [9], [10], [11], detecting movements of an object [12], [13], and secure communication [14], [15], continuously revolutionize the horizon. Such applications rely heavily on accurate measurements of the Channel State Information (CSI), which refers to the channel properties such as channel frequency responses of a communication link in a special frequency band. This information describes how a signal propagates from the transmitter to the receiver and represents the combined effect of, for example, scattering, fading, and power decay with distance. Theoretically, the frequency domain responses can also be transformed lossless to the time domain Power Delay Profile (PDP) through IFFT (Inverse Fast Fourier Transform). A PDP fully characterizes a multipath channel, and has been recently used for various motion- or location-based applications. As a result, accurate CSI measurements are of great significance to a wide variety of applications.

To obtain a CSI, commodity WiFi network interface cards (NICs) such as Intel 5300 [16] and Atheors AR9380 [17] can be easily used. Deriving accurate CSIs directly from such NIC readings, however, is challenging as the obtained CSI measurements describe not only channel properties in passband but also the signal processing circuit properties in baseband. For example, Fig. 1 illustrates both amplitude and phase errors in raw CSIs measured in six 20 MHz 802.11n bands in a typical indoor environment using Atheors AR9380 NICs. Previous studies [9], [14], [15], [18], [19] have pointed out the following sources of CSI measurement errors due to hardware imperfection in wireless signal processing, including power control uncertainty, packet detection delay (PDD), sampling frequency offset (SFO), carrier frequency offset (CFO), random initial phase offset, and phase ambiguity. The impacts of above error sources to CSI measurements are three-fold: 1) power control uncertainty causes a CSI amplitude offset; 2) packet detection delay and SFO, essentially equivalent to a time delay, cause CSI phase rotation errors; 3) the rest would respectively cause an identical CSI phase offset error on each measured sub-carriers. Consequently, these sources can only introduce linear phase errors expressed as a rotation error proportional to the sub-carrier index plus an offset in the measured CSI phases.

According to previous work [20], the CSI amplitude offsets in individual bands can be easily removed by averaging a sufficient number of CSI measurements obtained within the channel coherence time. As for CSI phase linear errors, several state-of-the-art strategies have been proposed. For example, a linear transform on raw CSI phases can be conducted [7], [13], in the way that the mean of phases on all sub-carriers is forced to zero, and the phase slope between the first sub-carrier and last sub-carrier is forced to

- H. Zhu, Y. Zhuo, and Q. Liu are with the Department of Computer Science and Engineering, Shanghai Jiao Tong University, Shanghai 200240, P.R. China. E-mail: {hongzi, zyw081285, lqh929289158}@sjtu.edu.cn.
- S. Chang is with the School of Computer Science and Technology, Donghua University, Shanghai 201620, P.R. China. E-mail: changshan@dhu.edu.cn.
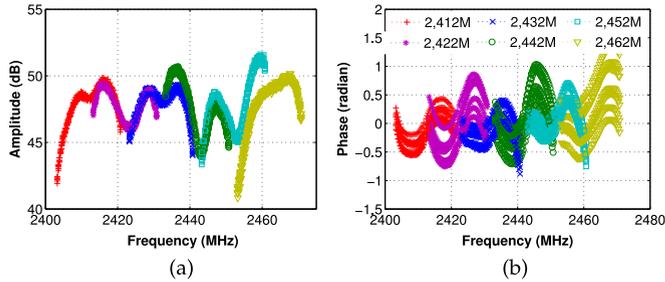
Fig. 1. (a) Raw CSI amplitudes obtained from six 20MHz 802.11n bands in a typical indoor environment. (b) The corresponding raw CSI phases.

zero too. Another example is to search a linear fitting [9], [15] and subtract the fitted linear function from the raw CSI phase. Recent work [19] obtains CSIs from different frequency bands, averages raw CSI phase measures from the same individual frequency band to mitigate the rotation error due to PDD, and search an identical rotation among individual frequency bands to compensate the rotation error due to SFO. All strategies above are based on an assumption that all the notable CSI phase errors except measurement noise are linear. In contrast, it is obvious to see from Fig. 1b that phases measured on sub-carriers especially for those at both ends of a band are severely distorted in a non-linear way, which suggests there exists an unknown source of non-linear CSI phase errors with commodity WiFi devices.

In this paper, we first introduce our previous work [21] on achieving accurate CSI phase measurements by conducting both extensive empirical study with commodity WiFi NICs and intensive analysis on the source of non-linear CSI phase errors. In addition to verifying those linear-error sources mentioned above, we find non-linear CSI phase errors are prevalent for commodity WiFi devices and identify that the root source of such non-linear errors stems from the IQ imbalance issue of direct down conversion receivers. We analyze the characteristics of non-linear CSI phase errors, and have the following two key observations: 1) non-linear CSI phase errors are rather stable over time and different received signal strength indication (RSSI) conditions; 2) such errors are sensitive to different frequency bands used between a transmission pair. Based on these observations, we propose a novel scheme to estimate parameters of our non-linear phase error model and eliminate non-linear CSI phase errors in multipath environments. Moreover, leveraging the insight that, when the channel is stable, the channel phase response for one specific frequency in passband should be the same, we propose to use the method of ordinary least squares on overlapping bands to further remove residual linear phase errors in each band.

To verify the efficacy of the proposed schemes for removing both non-linear and linear CSI phase errors, we carry out a case study and develop a *phase-improved* Splicer system, called *pi*-Splicer or π-Splicer, to incorporate above techniques on commodity Atheors 9580 NICs. We conduct extensive real-world experiments in three different indoor environments with light-of-sight and non-light-of-sight (NLOS) conditions to evaluate the derived CSIs in terms of smoothness at overlapping frequencies and stability of spliced CSIs. In addition, the derived CSIs are applied to an application of indoor distance ranging. Results demonstrate that accurate CSI phase measurements can be achieved,

which significantly improves the performance of CSI splicing and indoor distance ranging. In particular, the estimated distance errors can be greatly reduced by up to 5.7 times comparing to the results derived with the state-of-the-art CSI splicing scheme.

In the remainder of this paper, we first introduce some preliminary knowledge about the channel frequency response, the current signal processing design used in commodity WiFi devices and the reported CSI measurement error sources in Section 2. Section 3 elaborates our empirical studies on CSI measurements, where non-linear CSI phase errors are identified and analyzed. We then propose schemes to eliminate both non-linear and linear CSI phase errors in Section 4. We apply our schemes to the CSI splicing and indoor distance ranging and evaluate the performance in Section 5. Section 6 presents related work. We conclude and direct future work in Section 7.

2 PRELIMINARIES

2.1 Theoretical Foundation

According to [17], [22], the channel frequency response $h(f)$ for multipath scenario can be expressed as

$$h(f) = \sum_{l=1}^{N} \alpha_l \cdot e^{-j \cdot 2\pi \cdot f \cdot \tau_l}, \qquad (1)$$

where N is the total number of multipaths, α_l and τ_l represent the attenuation and the propagation delay of the signal through path l, respectively. For each CSI entry, the channel frequency responses for all sub-carriers and all transmission pairs are organized as one CSI matrix. Each frequency response is complex, so it can be expressed with amplitude and phase.

For single direct path scenario, since different sub-carriers in the same frequency band undergo the same time-of-flight, the phase difference between sub-carriers m and n can be expressed as

$$\Delta_{m,n} = -2\pi \cdot (f_m - f_n) \cdot \tau_1 \, mod \, 2\pi, \qquad (2)$$

where f_m and f_n are the frequency of sub-carriers m and n in passband.

2.2 Signal Processing at an 802.11 Receiver

A typical WiFi 2.4 GHz receiver with direct down conversion architecture is shown in Fig. 2. An incoming radio frequency (RF) a pair of quadrature sinusoidal signals to perform the so-called quadrature down conversion in order to get the in-phase (I) and the quadrature (Q) baseband signals. After that, a programmable gain filter/amplifiers (PGA) and an Analog-to-Digital convertor (ADC) are applied to the parallel I and Q branches. After sampling, the discrete time domain signal $r[n]$ is passed through the packet detector, which performs energy detection or correlation between $r[n]$ and a pre-defined 802.11 preamble pattern to confirm an incoming packet. Because the existence of CFO will seriously degrade the performance of OFDM, once the packet is detected, the CFO is estimated and corrected to minimize the effects of ICI in the later stages. The channel estimator estimates the instantaneous CSI and the
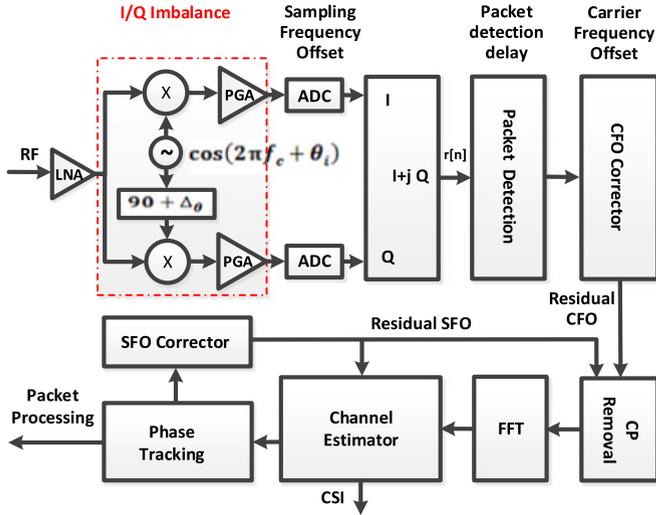
Fig. 2. Illustration of signal processing in 802.11n.

subsequent equalization module (not shown) acts as channel corrector to compensate attenuation and phase errors prior to the packet decoding. Note that, the extracted CSI characterizes not only the frequency response of the external wireless channel in passband, but also the frequency response of the inner circuit mainly in baseband.

2.3 Reported CSI Measurement Error Sources

Since we aim to sense the external environment with CSIs extracted from commodity WiFi NICs, in this paper, all frequency responses of the inner signal processing circuit are regarded as errors. Besides measurement noise, previous studies [6], [8], [9], [15], [16] have reported the sources of CSI measurement errors as follows.

Power Amplifier Uncertainty (PAU). Due to the resolution limitation of hardware, for example, 0.5dB for Atheros 9380, the total gain achieved from LNA and PGA cannot perfectly compensate the signal amplitude attenuation to the transmitted power level. The measured CSI amplitude equals to the compensated power level, mixed with a power amplifier uncertainty error, which causes a CSI amplitude offset.

Carrier Frequency Offset (CFO). The central frequencies of a transmission pair cannot be perfectly synchronized. The carrier frequency offset is compensated by the CFO corrector of the receiver, but due to the hardware imperfection, the compensation is incomplete. Signal still carries residual CFO, which leads to a time-varying CSI phase offset across sub-carriers.

Sampling Frequency Offset (SFO). The sampling frequencies of the transmitter and the receiver exhibit an offset due to non-synchronized clocks, which can cause the received signal after ADC a time shift with respect to the transmitted signal. After the SFO corrector, residual SFO leads to a rotation error. Because clock offsets are relatively stable within a short time (e.g., in the order of minutes [10]), such phase rotation errors are nearly constant.

Packet Detection Delay (PDD). Packet detection delay stems from energy detection or correlation detection which occurs in digital processing after down conversion and ADC sampling. Packet detection introduces another time shift with respect to the transmitted signal [13], [21], which leads to packet-varying phase rotation error.

PLL Phase Offset (PPO). The phase-locked loop (PLL) is responsible for generating the center frequency for the transmitter and the receiver, starting at random initial phase [8]. As a result, the CSI phase measurement at the receiver is corrupted by an additional phase offset.

Phase Ambiguity (PA). When examining the phase difference between two receiving antennas, recent work [14] validates a so called four-way phase ambiguity existence in Intel 5300 when working on 2.4 GHz. Generally speaking, if the phase difference between the first receiving antenna and the second antenna should be $\theta \in (0, \pi/2)$, the four-way phase ambiguity can lead the phase difference to be θ, $\theta + \pi/2$, $\theta - \pi/2$ or $\theta - \pi$. As for Atheros 9380, we similarly discover a two-way phase ambiguity. As a result, phase ambiguity will lead to another phase offset.

From the above known error sources, the measured CSI phases are mainly distorted with various phase ration errors and/or phase offset errors. For a transmission pair, the phase measurement $\phi_{(i, k)}$ for sub-carrier k in band i can be expressed as

$$\phi_{i,k} = \theta_{i,k} - 2\pi \cdot k \cdot f_s \cdot \delta_i + \beta_i + Z, \qquad (3)$$

where k ranges from -28 to 28 (index 0 is reserved for carrier frequency) in IEEE 802.11n for 20 MHz band width, $\theta_{(i, k)}$ denotes the true phase, δ_i is the timing offset at the receiver, including time shift due to PDD and SFO, f_s is the sub-carrier spacing between two adjacent sub-carriers (i.e., 312.5 KHz), β_i is the total phase offset, and Z is the additive white Gauss measurement noise. Note that, except for Z, other reported phase errors are linear with sub-carrier indexes.

3 IDENTIFYING NON-LINEAR CSI PHASE ERROR AND ITS ROOT SOURCE

In this section, we conduct empirical study on CSI measurements and describe the non-linear errors and their characteristics with respect to both amplitude and phase.

3.1 Observing Non-Linear CSI Phase Errors

In 802.11n, a channel sounding mechanism is defined, with which a transmitter can trigger CSI estimation at a receiver by setting an appropriate flag in the transmitted packet [23], [24]. We adopt Atheros AR9380 and Intel 5300 NICs, which support 802.11n with 20 MHz/40 MHz bands at the 2.4 GHz/5 GHz frequency bands and have three antennas on each NIC. In specific, we setup two pairs of HP desktops running Linux OS with one pair installed with Atheros AR9380 NICs and the other installed with Intel 5300 NICs. With the help of the open source software *hostapd*, we configure one desktop in each pair to acts as AP to transmit packets and the other one as the receiver to extract CSI measurements. We also modify the drivers of both NIC drivers so that receivers can report an estimated CSI to the user space once a packet is received. Packets in all experiments have the minimum payload (to ensure a short transmission delay, i.e., about 0.2 ms in our experiment). When working in a 20 MHz band with Atheros (Intel) NICs, there are 56 (30) complex numbers in one CSI measurement for each transmission pair.

We conduct an experiment in a typical indoor environment with the length and width of the room being 12 meters
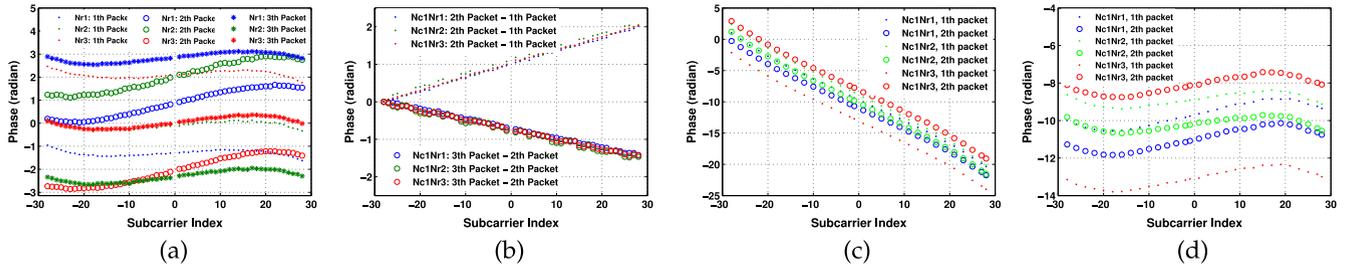
Fig. 3. (a) Three groups of unwrapped CSI phases measures from strong LOS scenario with Atheros AR9380. (b) The CSI phase differences of each transmission pair between two consecutive packets, with Nc1Nr1, Nc1Nr2, and Nc1Nr3 denoting transmitting pairs between the first antenna of the transmitter and the first, the second and the third antenna of the receiver, respectively. (c) Two unwrapped CSI phase measures between one transmission pair with Intel 5300 NICs. (d) The phase measures after compensating another phase rotation corresponding to a time shift of 200ns.

and 10 meters, respectively. We arrange the transmitter and the receiver in strong line-of-sight condition with distance of 0.5 meter, and make the transmitter to transmit with its first antenna, denoted as *Nc1*, with a fixed transmitting power of 5 dBm and the receiver to receive with all of its three antennas denoted as *Nr1*, *Nr2* and *Nr3* respectively. We collect CSIs when the environment is stable.

Fig. 3a illustrates three groups of unwrapped CSI phase measurements for three consecutive packets, with each group containing CSI phases for 1 by 3 transmission pairs. Intuitively, in such strong LOS scenarios, the direct path component dominates all multipath components in the total power of the received signal. According to (2), the ideal phases on different sub-carriers should be almost linear with the sub-carrier indexes. We observe, however, obvious non-linear distortions in all unwrapped phase measurements. We repeat such experiment in an indoor gymnasium with length of 50 meter and width of 30 meter, and get similar results. According to previous work [5], [19], if the wireless channel is stable, the unwrapped phase differences of two consecutive packets for the same transmission pair are almost linear. After removing the phase offset at sub-carrier #-28 from each CSI phase measurement, we calculate the CSI phase differences of each transmission pair between any two consecutive packets using the same CSIs in Fig. 3a and plot the results in Fig. 3b. It can be clearly seen that the unwrapped phase differences of two consecutive packets for the same transmission pair are almost linear with the sub-carrier index, indicating that the environment is quite stable. In addition, it also suggests that the non-linear CSI phase errors seem to be constant between different measurements.

We repeat the experiment except that we change to use Intel 5300 NICs and draw the unwrapped CSI phase measures of two packets in Fig. 3c. At the first glance, it seems that the CSI phases are pretty linear with sub-carrier indexes. According to previous work [25], the packet detection delay can span hundreds of nanoseconds for Intel 5300. After compensating 4 sampling periods, i.e., 200 ns, we plot the corrected CSI phases in Fig. 3d. It can be seen that the envelopes of phase measures are similar to Fig. 3a.

To further confirm the existence of non-linear CSI errors, we conduct more intensive measurements. In specific, we use a RF cable of 30 cm and an attenuator of 50 dB to connect the first radio chains of both the transmitter and the receiver. The transmitter sends 1,000 packets within three seconds each time with a fixed transmission power of 15 dBm in a 20 MHz band with a central frequency of 2,412 MHz. We random select 100 CSI measurements,

remove the mean from each CSI phase measurement, and plot the unwrapped CSI phases and the phase differences for any two consecutive phase measures in Fig. 4a and 4b, respectively. We have two main observations as follows: 1) the envelopes of unwrapped phases are not linear but symmetrical and analogous to some form of trigonometric function; 2) the phase differences of consecutive packets are linear with sub-carrier index, which makes one envelope easy to rotate to another. The default assumption that only notable linear phase error exists cannot hold and an unrevealed non-linear phase error exists, which cannot be mitigated through existing methods. To make matter worse, obviously this non-linear error is orders-of-magnitude higher than the ground truth[1] phase and thus non-negligible. We augment the CSI phase error model as

$$\phi_{i,k} = \theta_{i,k} + \varphi_{i,k} - 2\pi \cdot k \cdot f_s \cdot \delta_i + \beta_i + Z, \qquad (4)$$

where $\varphi_{i,k}$ denotes the non-linear error as a function of the sub-carrier index k in band i, with other parameters the same as in (3).

3.2   Root Source of Non-Linear CSI Phase Errors

Commodity WiFi 2.4 GHz receivers normally adopt the direct down conversion architecture as shown in Fig. 1. According to previous work [26], [27], there is a universal performance issue, named *IQ imbalance*, in the design of direct down conversion receivers. A direct conversion receiver uses two quadrature sinusoidal signals to perform the quadrature down conversion. This process requires shifting the local oscillator (LO) signal by 90 degrees to produce a quadrature sinusoidal component. When mismatches exist between the gain and phase of the two sinusoidal signals and/or along the two branches of down-conversion mixers, amplifiers, and low-pass filters, the quadrature baseband signals will be corrupted. Once I/Q imbalance exists, after sampling and FFT, the NIC would estimate and report an anamorphic CSI.

When there is only one path between a transmission pair, we assume the averaged phase measurement $\phi_{i,k}$ of subcarrier k in band i as

$$\phi_{i,k} = atan\left(\epsilon_{i,A} \cdot \frac{sin(2\pi \cdot f_s \cdot k \cdot \zeta + \epsilon_{i,\theta})}{cos(2\pi \cdot f_s \cdot k \cdot \zeta)}\right) - 2\pi \cdot f_s \cdot k \cdot \lambda + \beta_i, \quad (5)$$

---

1. With a 30cm RF cable, the ground truth of CSI phases is a line with the slope being about 0.002 rad/sub-carrier index.
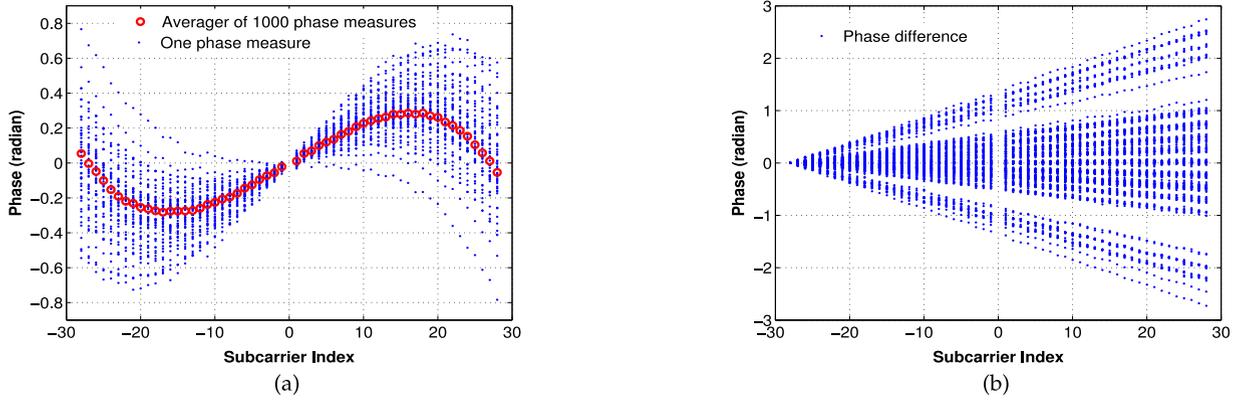
Fig. 4. (a) 100 CSI phase measurements in a 20MHz WiFi band at the 2.4GHz frequency band between a transmission pair obtained in a stable and approximate single direct path, with the mean of each measurement removed to zero. (b) The phase differences of 100 phase measures, after removing a particular phase offset respectively.

where $\epsilon_{i,A}$ and $\epsilon_{i,\theta}$ denote the gain mismatch and the phase mismatch for band i respectively due to the IQ imbalance problem, ζ is an unknown timing offset, λ is the equivalent timing delay caused by time-of-flight, PDD and SFO, and β_i is a phase offset error.

To verify the validity of (5), we then apply the least-square regression analysis to the average of the 1,000 CSIs measured via a short RF cable as described in above subsection. The significance of the regression is measured by the coefficient of determination r^2, defined as $r^2 \equiv 1 - \frac{\sum_i (y_i - \bar{y})^2}{\sum_i (y_i - f_i)^2}$, where y_i is the averaged CSI phase with mean $\bar{y}$ and f_i is the modeled/fitted value.

As shown in Fig. 5, the averaged CSI phase measurements are very well approximated ($r^2 > 0.998$) by the model in (5). We repeat this exercise in all bands and with all NICs and obtain similar results. As a result, we claim that the IQ imbalance problem is the root source of non-linear CSI phase errors.

3.3 Characteristics of Non-Linear Phase Errors

We study the characteristics of non-linear CSI phase errors and conduct more intensive CSI measurements. In specific, we use combinations of different attenuators of 30/40/50/60 dB and transmitting powers of 15/10/5 dBm to achieve various signal strength. In addition, the transmitter and receiver hop synchronously among six different bands once
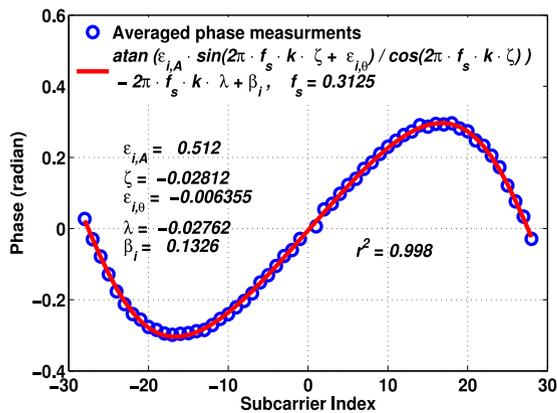

Fig. 5. Illustration of the least-square regression on the phases of an averaged CSI example.

1,000 CSIs are collected and averaged on one band. For each configuration, we repeat the data collection for 200 times in a duration of two weeks and for each time we conduct the least-square regression analysis to the averaged CSI to derive all parameters in (5).

Fig. 6 plots the derived parameters related to non-linear CSI phase errors. We have the following four main observations: 1) on a particular band and in a relatively stable environment, the gain mismatch $\epsilon_{i,A}$, the phase mismatch $\epsilon_{i,\theta}$ and the unknown time delay ζ are rather stable along time; 2) on a particular band but in different RSSI conditions, the gain mismatch $\epsilon_{i,A}$, the phase mismatch $\epsilon_{i,\theta}$ and the unknown time delay ζ slightly vary but are still stable as each parameter tends to fluctuate around a horizontal line as RSSI changes; 3) the phase mismatch $\epsilon_{i,\theta}$ is sensitive to the frequency bands as they diverge clearly when measured on different bands but in relatively stable RSSI conditions; 4) from Fig. 6d, it can be seen that the unknown time delay ζ is stable when changing bands and RF cables of different length, which indicates that ζ is independent of frequency bands and the time-of-flight of signal.

Fig. 7 plots the derived parameters related to linear CSI phase errors. We have the following four main observations: 1) the timing delay δ_i introduced by PDD and SFO in (4)[2] is independent of frequency bands and RSSI conditions; 2) on a particular band and in a relatively stable RSSI environment, the timing delay δ_i follows a nonzero-mean Gaussian distribution; 3) the variance of the Gaussian distribution of δ_i is large; 4) the phase offset error β_i is analogous to the timing delay δ_i except the mean of its Gaussian distribution is zero.

4 PERCEIVING ACCURATE CSI PHASE MEASUREMENTS

4.1 Removing Non-Linear Phase Errors

From the above study, we have one key observation that non-linear CSI phase errors caused by IQ imbalance are relatively stable over time and various RSSI conditions but sensitive to frequency bands. If the parameters of $\epsilon_{i,A}$, $\epsilon_{i,\theta}$ and ζ are known, non-linear phase errors can be removed. On one hand, if there is only one dominant path between a

---

2. δ_i can be derived by subtracting the known time-of-flight from the equivalent timing delay λ, when only the direct path exists.

(a) The gain mismatch $\epsilon_{i,A}$ (b) The phase mismatch $\epsilon_{i,\theta}$ (c) The timing offset ζ
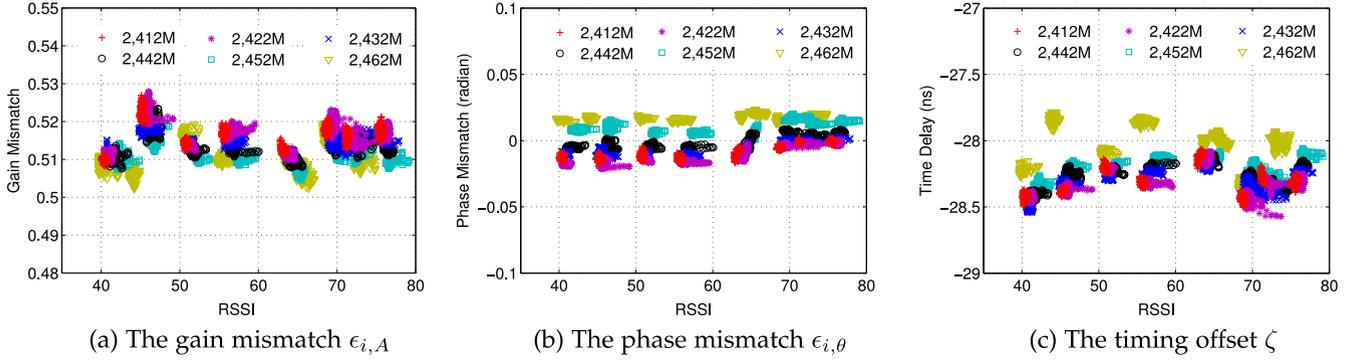
Fig. 6. Estimates of parameters related to non-linear CSI phase errors, obtained in different RSSI conditions and six bands.

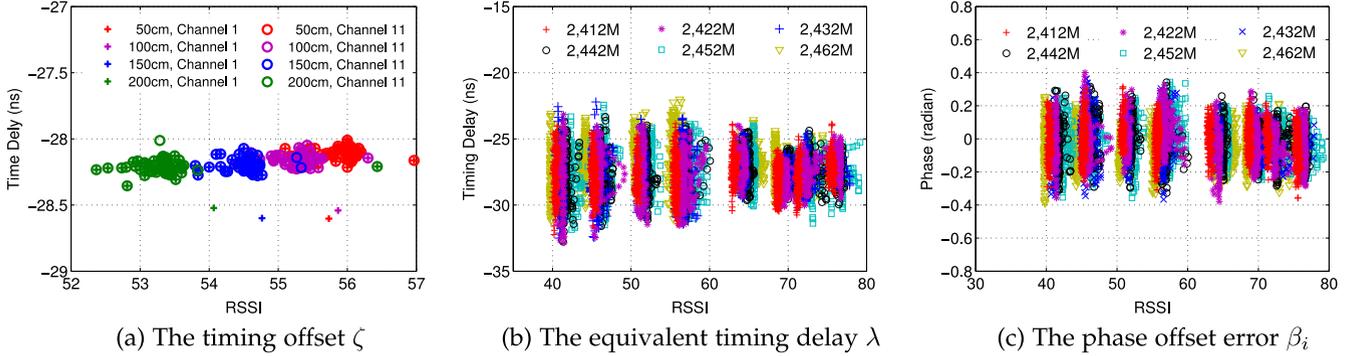(a) The timing offset ζ (b) The equivalent timing delay λ (c) The phase offset error β_i

Fig. 7. (a) The timing offset ζ is further studied with different lengths of RF cables (i.e., time-of-flight). (b) (c) Estimates of parameters related to linear CSI phase errors, obtained in different RSSI conditions and six bands.

transmission pair, least-square regression analysis as described in Section 3.2 can be conducted but in real world multipath is inevitable. One straightforward method is to connect the transmission pair via an RF cable but it is infeasible in most cases. On the other hand, if a measured CSI phases can perfectly fit the model in (5), it means that either only one dominant path exists (e.g., in a strong LOS and weak multipath environment) or multipath is counteracted.

With this inference, we propose to conduct a *utility test* on raw CSIs and a CSI is said to be positive if it passes the test. In the test, we apply the least-square regression analysis to the phases of a CSI as described in Section 3.2. In specific, the condition for this CSI to pass the test is that the significance of the regression measured by the coefficient of determination r^2 is larger than a threshold. In practice, we set this threshold to 0.995. We find that positive CSIs can always be obtained when putting the transmission pair in a strong LOS and weak multipath environment. With sufficient positive CSIs, parameters of $\epsilon_{i,A}$, $\epsilon_{i,\theta}$ and ζ associated with specific bands can be accurately estimated without RF cables and used to remove future non-linear CSI phase errors.

4.2 Removing Linear Phase Errors

From previous analysis in Section 3.3, though the linear (or rotation) CSI phase errors introduced by PDD and SFO are Gaussian distributions, due to large variance, it is infeasible to get the mean by averaging a small number of CSIs measured within the channel coherence time. As a result, each averaged CSI still has its own residual phase rotation error.

In order to eliminate phase rotation errors, we leverage the key insight that, given that the wireless channel is stable, the channel phase response for one specific frequency in

passband should be the same even when it is measured from different bands. As illustrated in Fig. 8, suppose there are M overlapping subcarriers between band i and band j both of which contain N non-zero indexed subcarriers exposed in the CSI measurements. The $\theta_{i,\frac{N}{2}-M+s}$ and $\theta_{j,-\frac{N}{2}+s-1}$, for $s \in [1, M]$, should be identical. According to (4), the measurement noise Z can be ignored for averaged CSIs and we have

$$
\begin{aligned}
\phi_{i,\frac{N}{2}-M+s} - \varphi_{i,\frac{N}{2}-M+s} + 2\pi \cdot \left(\frac{N}{2} - M + s \right) \cdot f_s \cdot \delta_i - \beta_i = \\
\phi_{j,-\frac{N}{2}+s-1} - \varphi_{i,-\frac{N}{2}+s-1} + 2\pi \cdot \left(-\frac{N}{2} + s - 1 \right) \cdot f_s \cdot \delta_j - \beta_j.
\end{aligned}
\tag{6}
$$

Given that $\phi_{i,\frac{N}{2}-M+s}$ and $\phi_{j,-\frac{N}{2}+s-1}$ are averaged CSI phases and the non-linear phase errors $\varphi_{i,\frac{N}{2}-M+s}$ and $\varphi_{i,-\frac{N}{2}+s-1}$ can be estimated, there are only 4 unknown parameters, i.e., δ_i, β_i, δ_j, and β_j for M equations. For overdetermined equations (i.e., M is larger than 4 for commodity WiFi devices), we adopt the method of ordinary least
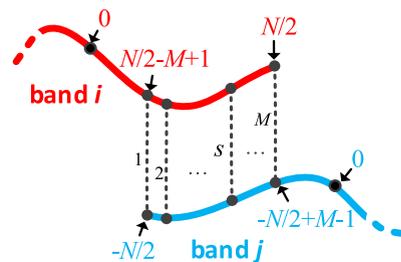

Fig. 8. Illustration of overlapping frequencies in two bands.

squares (OLS) to find an approximate solution. After compensating with both non-linear and linear phase errors, a good estimation of the channel phase response in a band i, i.e., $\theta_{i,k}$, can be obtained by calculating the $\phi_{i,k} - \varphi_{i,k} + 2\pi \cdot k \cdot f_s \cdot \delta_i - \beta_i$ for not only those overlapping subcarriers but also non-overlapping subcarriers.

5 CASE STUDY: CSI SPLICING

5.1 Overview

As the resolution of the PDP derived from one single 20 MHz band with commodity WiFi devices is only approximate 15 m, which seriously limits the performance of PDP-based upper-layer applications such as localization, object tracking and gesture recognition. Splicer [19] is the first scheme to splice frequency response of several individual bands so as to derive a higher resolution PDP. In Splicer, to splice CSI amplitudes in different bands, CSI amplitudes measured on individual bands are averaged. In order to splice CSI phases in different bands, Splicer first compensates PDD phase errors on each band by averaging a finite number of CSI phases measured in that band, with the assumption that the time delay caused by packet detection follows a zero-mean Gaussian distribution. After that, Splicer searches for a global rotation compensation and applies to all bands to remove the SFO phase errors. The stopping criteria of such search is to make the PDP derived from individual bands have the highest similarity.

There are three main factors that would degrade the performance of Splicer. First, in the SFO phase error removal, Splicer relies on the similarity of PDPs derived from single WiFi bands. Due to the limited bandwidth of such bands, the resolution of the derived PDPs is low and inaccurate. Second, the global rotation compensation is calculated based on pairwise rotation compensations between two overlapping bands. When pairwise rotation compensations disagree with each other, the global rotation compensation is not optimal. Last, as the non-linear phase errors are not considered in Splicer, the spliced phases and the resulted PDP are not accurate.

5.2 The π-Splicer Scheme

We propose a *phase-improved* Splicer scheme, called *pi-Splicer* or *π-Splicer*, which enhances Splicer in terms of phase splicing in two ways as follows. First, the non-linear phase error factors, i.e., $\epsilon_{i,A}$, $\epsilon_{i,\theta}$ and ζ as in (5) are first estimated according to the scheme proposed in Section 4.1. With the studied non-linear phase error model, non-linear phase errors can be removed from averaged CSIs measured in each band, resulting non-linear-error-free CSIs. For example, Fig. 9a plots seven groups of averaged raw CSIs of six bands and Fig. 9b shows the corresponding results with non-linear phase errors removed. Second, we then apply the linear phase error removal scheme proposed in Section 4.2 to those non-linear-error-free CSIs among all bands to be spliced. With more restrictive conditions available to (6), the least square solution can achieve the global optimal among all bands. For example, in Fig. 9c, after removing linear phase errors, CSI phases over different bands can be smoothly spliced. After the above two steps, a final spliced CSI phases can be obtained by averaging

(a) Raw CSI phases   (b) Non-linear errors removed

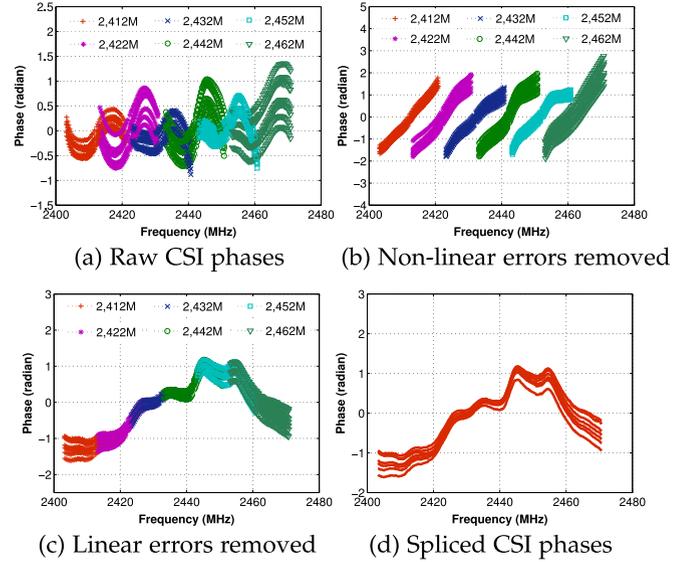(c) Linear errors removed   (d) Spliced CSI phases

Fig. 9. The CSI phases in each stage during splicing.

phases in overlapping frequencies. Fig. 9d illustrates the final spliced phases of the raw CSIs in Fig. 8a.

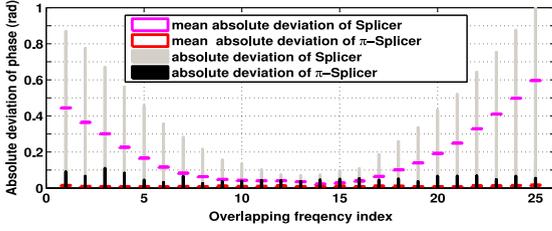## 5.3 Performance Evaluation

Methodology. We use Atheors AR9380 NICs and collect CSIs on six 20 MHz bands (i.e., band 1, 3, 5, 7, 9 and 11) at the 2.4 GHz frequency bands. We fix the transmitter and change the position of the receiver randomly selected from 10 LOS locations and 10 NLOS locations, respectively, in three different indoor environments, i.e., a 12 m × 10 m laboratory room, a 50 m × 3 m corridor and a gym. At each location, after collecting a batch of 20 CSIs within 4 ms on one band, the transmission pair both switch to another band within 5 ms. It takes about 50 ms[3] to iterate all considered bands and a group of CSIs over all bands can be obtained. We repeat the iteration for 60 times (about 3s) at one location and then move the receiver to the next location. In order to verify the stability of PDPs derived from CSIs, we keep the environment as static as possible. The batches of 20 CSIs collected on each individual bands in each group are first averaged.

We then conduct the utility tests for all averaged CSIs collected in LOS conditions with the threshold of the coefficient of determination r^2 set to 0.995. For each band, we randomly select 50 positive averaged CSIs to learn the empirical values of $\epsilon_{i,A}$, $\epsilon_{i,\theta}$ and ζ and take the average for each parameter. After that ,the learned $\epsilon_{i,A}$, $\epsilon_{i,\theta}$ and ζ are used to remove non-linear phase errors of averaged CSIs measured on the corresponding band i. Finally, the OLS method is adopted to find the optimal solution of all δ_i and β_i and compensate phase rotation errors for each group of averaged CSIs of six bands. In addition, we take the same procedure to splice CSI amplitudes as introduced in Splicer and derive high-resolution PDPs with spliced CSI amplitudes and phases.
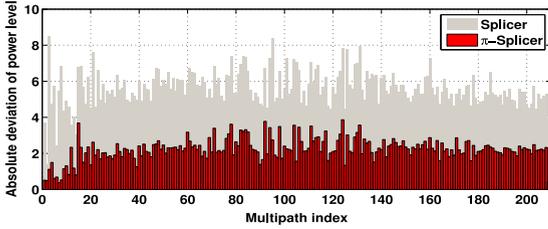
CSI Splicing. We evaluate and compare the performance of Splicer and our π-Splicer using the following two metrics:

- *Phase differences at overlapping frequencies.* It is known that the phase responses should be identical for

---

3. The channel coherence time when human mobility exists is around 50ms [19].

(a) Statistics of standard deviations of phase difference on overlapping frequencies

(b) Standard deviations of power level in an example location

Fig. 10. Performance of splicer and π-splicer.

subcarriers of the same frequency in two bands. For a group of six corrected CSIs, there are five overlapping frequency bands with each having 25 overlapping subcarriers, i.e., $M = 25$ as in Fig. 8. For each $s \in [1, 25]$, we calculate the difference of two corrected phases in each overlapping band of a group before splicing and calculate the standard deviation.

- *Stability of PDPs obtained in static environments.* A set of PDPs are accurate and obtained in a static environment, they should be very similar if not identical. For each location in our experiment, we calculate the standard deviation of the power levels for each multipath over all 60 PDPs derived from corresponding groups of CSIs.

Fig. 10a depicts the mean and the range of standard deviations calculated over all groups of CSIs and all locations. Its clear that the mean, the minimal and the maximal deviations of π-Splicer are all much smaller than these of the original Splicer. In addition, it is interesting to see that the original Splicer prefers to align phases at subcarriers in the middle of overlapping bands, leaving subcarriers at both ends badly aligned. In contrast, π-Splicer can align all overlapping frequencies perfectly.

Fig. 10b depicts the standard deviation of power levels over each multipath in a NLOS condition. It can be seen that the PDPs derived by π-Splicer are more stable than those derived by the original Splicer. Moreover, we also notice that the standard deviations of the first 12 paths is just about 1 dB for π-Splicer. On one hand, the small deviation indicates the environment is static. On the other hand, we explain that this 1 dB deviation is because of the small amplitude differences (around 1 dB) among spliced CSIs.

Figs. 11 and 12 plot the cumulative distribution functions (CDFs) of the standard deviations of power levels for the direct path, the first 5, 10, and 20 paths among all LOS conditions and among all NLOS conditions, respectively. It can be seen that in all cases the PDPs derived by π-Splicer are more stable comparing with the original Splicer. Particularly, the standard deviations for the direct path are less than 1.5 dB. The superior stability of PDPs can greatly
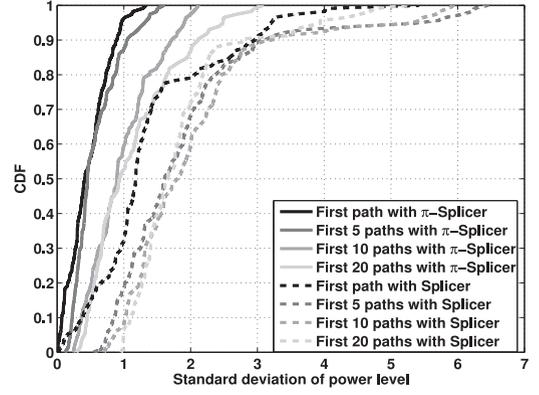

Fig. 11. CDFs of standard deviation of power levels in LOS conditions.

facilitate applications such as gesture recognition [2], [3]. Furthermore, it is clear to see that the PDPs derived with Splicer is less stable in NLOS conditions. In contrast, π-Splicer is superior to Splicer in deriving stable PDPs under all channel conditions.

Indoor Distance Ranging. Besides the angle-of-arrival (AoA) information [28], [29], time-of-flight (ToF) information can be used in indoor localization. We demonstrate the efficacy of pi-Splicer in the indoor ranging application. With pi-Splicer, we can obtain more accurate CSIs for a wider band within the coherence time. After IFFT operation, more accurate and higher resolution PDPs can be derived, which can significantly improve the performance of upper-layer applications. In this experiment, we demonstrate the efficacy of pi-Splicer by applying the spliced CSIs over six WiFi channels to indoor distance ranging. According to CUPID [30], it is reasonable to estimate the indoor distance d between a transmitter and a receiver as follows,

$$d = 10^{(P_d - P_0)/10\gamma}, \tag{7}$$

where P_0 and P_d are the receivenergies of the direct path (EDP) at the distance of 1m and dm from the transmitter, γ is the path loss exponent which is determined by the propagation characteristics. As in CUPID and Splicer, EDP is approximated as the energy of the first component of a PDP, and the fitting value of γ can be learned. Distance estimation based on EDP is more robust than that based on RSSI since it is much less susceptible to multipath reflections, especially when the EDP is derived from an accurate and high-resolution PDP.
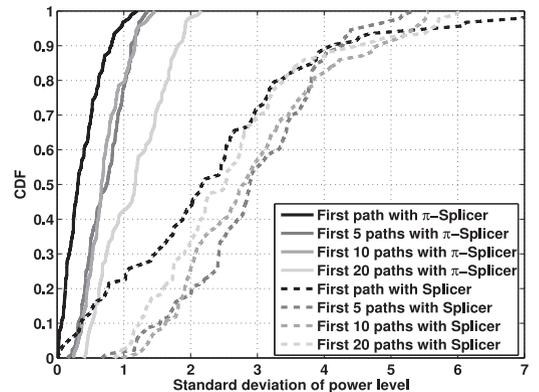

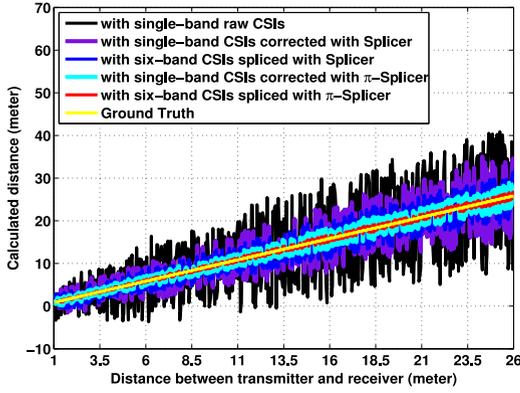Fig. 12. CDFs of standard deviation of power levels in NLOS conditions.

Fig. 13. Calculated distance versus real distance between the transmitter and the receiver.

Fig. 14. CDFs of ranging errors using difference CSIs.

We consider the 100 m × 3 m indoor corridor as it is the worst indoor scenario because of strong multipath reflections. Analogous to above experiment setting, we fix the transmitter at a random location in the corridor and change the position of the receiver at a distance from the transmitter, ranging from 1 m to 26 m at an interval of 0.25 m. At each location, after collecting a batch of 60 CSIs on one band, the transmission pair both switch to another band until all six bands are iterated. We repeat the iteration for 20 times at one location and then move the receiver to the next location. We also move the transmitter at five different locations and repeat the CSI measurement at each location.

For each location of the transmitter and each location of the receiver, we can obtain five distinct CSI measurements, i.e., single-band raw CSIs, six-band spliced CSIs derived with Splicer, single-band CSIs corrected with Splicer, six-band spliced CSIs derived with π-Splicer, and single-band CSIs corrected with π-Splicer. In particular, to obtain spliced CSIs, we adopt the same procedure as in the above experiment to splice each group of averaged CSIs of six bands, using both Splicer and π-Splicer schemes. Single-band corrected CSIs are those modified single-band CSIs after removing phase and amplitude errors using Splicer and π-Splicer, respectively. Given a CSI, after IFFT operation, we can derive the corresponding PDP and the approximate value of EDP and calculate the distance between the transmitter and the receiver according to (7). As a result, we calculate the distance between the transmitter and the receiver using different CSI measurements.

Fig. 13 plots the calculated distance as a function of real distance between the transmitter and the receiver. It can be seen that ranging with single-band raw CSIs is very unreliable. After correcting raw CSI errors with Splicer, the calculated distance results still diverge a great deal from the ground truth. In contrast, the estimated distance is very close to the ground truth using spliced CSIs derived by π-Splicer. It can also be seen that even if single-band CSIs corrected with π-Splicer are used, the estimated distance is more accurate than using spliced six-band CSIs corrected with Splicer. Fig. 14 shows the detailed statistical ranging errors for using different CSIs. It is clear to see that, after compensation with Splicer, the median and the maximum errors can be reduced from 12.23 m and 30.10 m (ranging with single-band raw CSIs) to 4.77 m and 19.21 m, respectively, whereas they can be dramatically reduced to 0.83 m
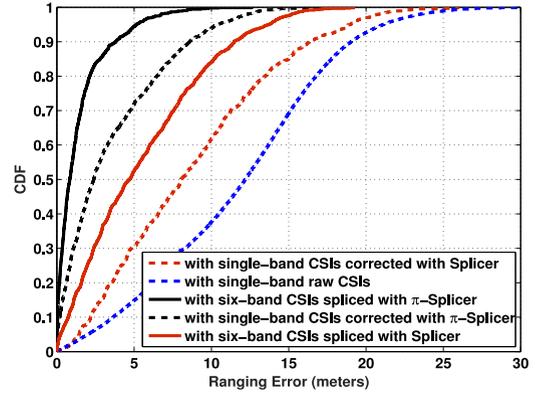
and 12.63 m, respectively, after correction with π-Splicer. The performance gain of π-Splicer not only stems from using CSIs of a broader band (i.e., PDPs of higher resolution) but more accurate CSI and PDP measurement.

6 RELATED WORK

6.1 Reported CSI Phase Errors

Besides measurement noise, prior studies also notice that the CSIs reported by WiFi NICs contain phase errors introduced by hardware. Previous studies [15], [18] explicitly point out SFO can cause a phase rotation error, and other studies [7], [8], [9], [10], [13], [19], [27] concern this rotation phase error too. Another phase rotation error can be caused by PDD [24], [31], [32], and studies [7], [8], [10], [13], [19] pay much attention to its existence. The authors of work [18] give a good description of the phase offset error caused by CFO, and points out the residual CFO is small after CFO corrector clearly. Recent work [8] observes and tries to mitigate a phase offset error caused by PPO. Another phase offset error due to PA is first validated by most recent work [14] in the using of Intel 5300, we observe this error exists similarly in Atheros 9380. However, all above phase errors are linear with sub-carrier indexes.

6.2 CSI Phase Calibration

As for CSI phase linear error, to the state of art, there are following strategies: Previous studies including [7], [10] recommend to perform a linear transform on the raw CSI phase. After transforming, both the mean of one phase measure and the phase slope between the first sub-carrier and last sub-carrier are forced to zero. After the transformation, the CSI phase measure can be used as fingerprint for some applications. However, such a brute transform just adds or subtracts another linear error. Studies [9], [13] search a linear fitting and subtract the fitting linear from the raw CSI phase. However, its common to over subtraction. Mega-MIMO aims to explicitly correct linear phase errors [27]. However, it requires both nanosecond-level synchronization and the access to the raw signal at PHY layer, which are not available on commodity NICs. Splicer [19] obtains CSIs from different frequency bands, averages raw CSI phase measures for the same individual frequency band expecting to mitigate the rotation error due to the PDD to same level, and cluster an identical rotation to compensate all phase measures from different bands. However, its

almost impossible to collect sufficient CSIs within the restriction of strict coherence time to guarantee the residua rotation error to be the same level. In order to remove random initial phase offset, the authors in work [8] propose to collect and process CSIs both from the transmitter and receiver for the same instant. However, even if CSIs can be collected at the instant, there is no guarantee for total phase offset error to be the same. All strategies above are designed for kinds of linear error, and none of them can eliminate rotation phase error well. Meanwhile, they are all based on an assumption that all the notable phase errors except measurement noise are linear with subcarrier indexes.

7   CONCLUSION AND FUTURE WORK

In this paper, we focus on obtaining accurate CSI phase measurements with commodity WiFi devices. Non-linear phase errors caused by the IQ imbalance issue are identified. In addition, such errors are independent of time and channel conditions but sensitive to frequency bands. We propose two novel schemes to remove non-linear CSI phase errors and residual phase rotation errors in indoor multipath environment. A case study of applying the proposed schemes in CSI splicing and indoor distance ranging is conducted. Results of extensive real-world experiments in various indoor environments demonstrate that accurate CSI phase measurements can be achieved, which significantly improves the performance of CSI splicing and indoor distance ranging.

This is an on-going research and system effort in sensorless sensing with WiFi. Following the current work, we have a lot of more exciting yet challenging topics ahead. One of these topics is whether improved CSI measurement can revolutionize mobile sensing applications such as gesture recognition and context perception. We will investigate the performance improvement of existing schemes when applying π-Splicer as the corner stone to obtain CSIs. Next, based on our prototype testbed, we will validate our design and study its performance in more complex indoor environments.

REFERENCES

[1] F. Adib and D. Katabi, "See through walls with Wi-Fi!" in *Proc. ACM SIGCOMM*, 2013, pp. 75–86.
[2] L. Sun, S. Sen, D. Koutsonikolas, and K.-H. Kim, "WiDraw: Enabling hands-free drawing in the air on commodity WiFi devices," in *Proc. 21st Annu. Int. Conf. Mobile Comput. Netw.*, 2015, pp. 77–89.
[3] G. Wang, Y. Zou, Z. Zhou, K. Wu, and L. M. Ni, "We can hear you with Wi-Fi!" in *Proc. 20th Annu. Int. Conf. Mobile Comput. Netw.*, 2014, pp. 593–604.
[4] Q. Pu, S. Gupta, S. Gollakota, and S. Patel, "Whole-home gesture recognition using wireless signals," in *Proc. 19th Annu. Int. Conf. Mobile Comput. Netw.*, 2013, pp. 27–38.
[5] Z. Zhou, Z. Yang, C. Wu, W. Sun, and Y. Liu, "LiFi: Line-of-sight identification with WiFi," in *Proc. IEEE INFOCOM*, 2014, pp. 2688–2696.
[6] Z. Zhou, et al., "WiFi-based indoor line-of-sight identification," *IEEE Trans. Wireless Commun.*, vol. 14, no. 11, pp. 6125–6136, Nov. 2015.

[7] C. Wu, Z. Yang, Z. Zhou, K. Qian, Y. Liu, and M. Liu, "PhaseU: Real-time LOS identification with WiFi," in *Proc. IEEE INFOCOM*, 2015, pp. 2038–2046.
[8] D. Vasisht, S. Kumar, and D. Katabi, "Decimeter-level localization with a single WiFi access point," in *Proc. 13th Usenix Conf. Networked Syst. Des. Implementation*, 2016, pp. 165–178.
[9] M. Kotaru, K. Joshi, D. Bharadia, and S. Katti, "SpotFi: Decimeter level localization using WiFi," in *Proc. Conf. Special Interest Group Data Commun.*, 2015, pp. 269–282.
[10] S. Sen, B. Radunovic, R. R. Choudhury, and T. Minka, "You are facing the Mona Lisa: Spot localization using PHY layer information," in *Proc. 10th Int. Conf. Mobile Syst., Appl. Services*, 2012, pp. 183–196.
[11] Y. Jin, W.-S. Soh, and W.-C. Wong, "Indoor localization with channel impulse response based fingerprint and nonparametric regression," *IEEE Trans. Wireless Commun.*, vol. 9, no. 3, pp. 1120–1127, Mar. 2010.
[12] C. Han, K. Wu, Y. Wang, and L. M. Ni, "WiFall: Device-free fall detection by wireless networks," in *Proc. IEEE INFOCOM*, 2014, pp. 271–279.
[13] Y. Wang, J. Liu, Y. Chen, M. Gruteser, J. Yang, and H. Liu, "E-eyes: Device-free location-oriented activity identification using fine-grained WiFi signatures," in *Proc. 20th Annu. Int. Conf. Mobile Comput. Netw.*, 2014, pp. 617–628.
[14] A. Tzur, O. Amrani, and A. Wool, "Direction finding of rogue Wi-Fi access points using an off-the-shelf MIMO-OFDM receiver," *Phys. Commun.*, vol. 17, pp. 149–164, 2015.
[15] S. Jana and S. K. Kasera, "On fast and accurate detection of unauthorized wireless access points using clock skews," *IEEE Trans. Mobile Comput.*, vol. 9, no. 3, pp. 449–462, Mar. 2010.
[16] Linux 802.11n CSI tool, Website, 2016. [Online]. Available: http://dhalperi.github.io/linux-80211n-csitool/installation.html
[17] Y. Xie, Atheros CSI tool, Website, 2016. [Online]. Available: http://pdcc.ntu.edu.sg/wands/Atheros/
[18] J. K. Tan, "An adaptive orthogonal frequency division multiplexing baseband modem for wideband wireless," Master's thesis, Dept. Electr. Eng. Comput. Sci., Massachusetts Inst. Technol., 2006.
[19] Y. Xie, Z. Li, and M. Li, "Precise power delay profiling with commodity WiFi," in *Proc. 21st Annu. Int. Conf. Mobile Comput. Netw.*, 2015, pp. 53–64.
[20] V. P. G. Jimenez, M. J. F.-G. Garcia, F. J. G. Serrano, and A. G. Armada, "Design and implementation of synchronization and AGC for OFDM-based WLAN receivers," *IEEE Trans. Consum. Electron.*, vol. 50, no. 4, pp. 1016–1025, Nov. 2004.
[21] Y. Zhuo, H. Zhu, H. Xue, and S. Chang, "Perceiving accurate CSI phases with commodity WiFi devices," in *Proc. IEEE INFOCOM*, 2017, pp. 1–9.
[22] T. S. Rappaport, et al., *Wireless Communications: Principles and Practice*. Englewood Cliffs, NJ, USA: Prentice Hall PTR, 1996, vol. 2.
[23] *IEEE 802.11n-2012 standard*. 2012, Website, 2016. [Online]. Available: http://standards.ieee.org/findstds/standard/802.11n-2012.html
[24] H. Rahul, H. Hassanieh, and D. Katabi, "SourceSync: A distributed wireless architecture for exploiting sender diversity," in *Proc. ACM SIGCOMM*, 2010, pp. 171–182.
[25] K.-Y. Sung and C.-C. Chao, "Estimation and compensation of I/Q imbalance in OFDM direct-conversion receivers," *IEEE J. Signal Process.*, vol. 3, no. 3, pp. 438–453, Jun. 2009.
[26] M. Petit and A. Springer, "Analysis of a properness-based blind adaptive I/Q filter mismatch compensation," *IEEE Trans. Wireless Commun.*, vol. 15, no. 1, pp. 781–793, Jan. 2016.
[27] H. Rahul, S. S. Kumar, and D. Katabi, "MegaMIMO: Scaling wireless capacity with user demands," in *Proc. ACM SIGCOMM*, 2012.
[28] J. Xiong and K. Jamieson, "ArrayTrack: A fine-grained indoor location system," in *Proc. 10th USENIX Conf. Networked Syst. Des. Implementation*, 2013, pp. 71–84.
[29] K. Qian, C. Wu, Z. Yang, Z. Zhou, X. Wang, and Y. Liu, "Tuning by turning: Enabling phased array signal processing for WiFi with inertial sensors," in *Proc. 35th Annu. IEEE Int. Conf. Comput. Commun.*, 2016, pp. 1–9.
[30] S. Sen, J. Lee, K.-H. Kim, and P. Congdon, "Avoiding multipath to revive inbuilding WiFi localization," in *Proc. 11th Annu. Int. Conf. Mobile Syst., Appl. Services*, 2013, pp. 249–262.
[31] J. Gjengset, J. Xiong, G. McPhillips, and K. Jamieson, "Phaser: Enabling phased array signal processing on commodity WiFi access points," in *Proc. 20th Annu. Int. Conf. Mobile Comput. Netw.*, 2014, pp. 153–164.
[32] L. He, et al., "ESync: An energy synchronized charging protocol for rechargeable wireless sensor networks," in *Proc. 15th ACM Int. Symp. Mobile Ad Hoc Networking Comput.*, 2014, pp. 247–256.

Hongzi Zhu received the PhD degree in computer science from Shanghai Jiao Tong University, in 2009. He was a post-doctoral fellow in the Department of Computer Science and Engineering, Hong Kong University of Science and Technology and the Department of Electrical and Computer Engineering, University of Waterloo, in 2009 and 2010, respectively. He is now an associate professor in the Department of Computer Science and Engineering, Shanghai Jiao Tong University. His research interests include vehicular networks, mobile sensing, and computing. He received the Best Paper Award from IEEE Globecom 2016. He is a member of the IEEE Computer Society and IEEE Communication Society. For more information, please visit http://lion.sjtu.edu.cn.

Yiwei Zhuo received the BS degree from the Department of Electronic Engineering, Xiamen University, in 2009, and the master's degree in computer science and engineering from Shanghai Jiao Tong University, in 2017. His research interests include pervasive computing, wireless network, and sensor networks.

Qinghao Liu received the BS degree from the Department of Computer Science and Engineering, Shanghai Jiao Tong University, in June 2018. His research interests include pervasive computing, wireless network, and mobile sensing.

Shan Chang received the BS degree in computer science and technology from the Xián Jiaotong University, in 2004 and the PhD degree in computer software and theory from Xián Jiaotong University, in 2013. Since 2013, she has been an associate professor with the Department of Computer Science and Technology at Donghua University. From 2009 to 2010, she was a visiting scholar in the Department of Computer Science and Engineering, Hong Kong University of Science and Technology. She was also a visiting scholar in the BBCR Research Lab, Electrical and Computer Engineering Department, University of Waterloo, from 2010 to 2011. Her research interests include security and privacy in mobile networks and wireless sensor networks. She is a member of the IEEE Computer Society and IEEE Communication Society.

▷ **For more information on this or any other computing topic, please visit our Digital Library at** www.computer.org/publications/dlib.